

Nature of Five-Coordinated Al in γ -Al₂O₃ Revealed by Ultra-High-Field Solid-State NMR

Zhenchao Zhao, Dong Xiao, Kuizhi Chen, Rui Wang, Lixin Liang, Zhengmao Liu, Ivan Hung, Zhehong Gan, and Guangjin Hou*



Cite This: *ACS Cent. Sci.* 2022, 8, 795–803



Read Online

ACCESS |



Metrics & More

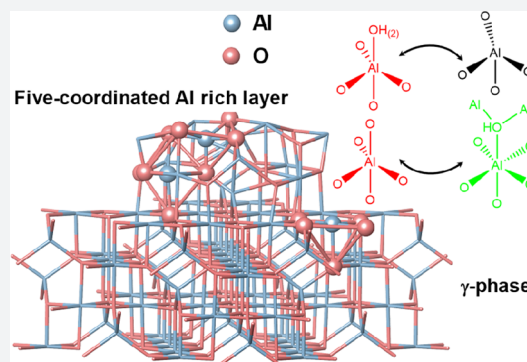


Article Recommendations



Supporting Information

ABSTRACT: Five-coordinated Al_s (Al(V)) on the surface of aluminas play important roles when they are used as catalysts or catalyst supports. However, the comprehensive characterization and understanding of the intrinsic structural properties of the Al(V) remain a challenge, due to the very small amount in commonly used aluminas. Herein, the surface structures of γ -Al₂O₃ and Al(V)-rich Al₂O₃ nanosheets (Al₂O₃-NS) have been investigated and compared in detail by multinuclear high-field solid-state NMR. Thanks to the high resolution and sensitivity of ultra-high-field (up to 35.2 T) NMR, the arrangements of surface Al_s were clearly demonstrated, which are substantially different from the bulk phase in γ -Al₂O₃ due to the structure reconstruction. It reveals for the first time that most of the commonly observed Al(V)s tend to exist as aggregated states on the surface of γ -Al₂O₃, like those in amorphous Al₂O₃-NS liable to structure reconstruction. Our new insights into surface Al(V) species may help in understanding the structure–function relationship of alumina.



INTRODUCTION

Transition aluminas with different structures and morphologies have been widely used as catalytic materials. As a typical alumina with high surface area and thermal stability, γ -Al₂O₃ has shown extensive applications in hydrodesulfurization, syngas to methanol, DeNO_x, and propane dehydrogenation reactions as industrial catalyst supports.^{1,2} The intrinsic Lewis acid sites (three-, four-, and five-coordinated Al) in γ -Al₂O₃ confer them with good acid catalytic properties for alcohol dehydration, olefin isomerization reactions, etc.¹ Because of its important practical applications, extensive studies on the structure of surface Al and hydroxyl species have been carried out utilizing infrared spectroscopy (IR), solid-state NMR spectroscopy, high-resolution transmission electron microscopy (TEM), temperature-programmed desorption, as well as theoretical calculations, to get a deeper understanding of the active sites for catalytic reactions and anchor sites when they are used as catalysts or catalyst supports.^{3–10} Nevertheless, the intrinsic low crystallinity makes detailed structural characterization of Al on the surface of γ -Al₂O₃ at the atomic level extremely challenging.^{11–13} Five-coordinated Al (Al(V)), claimed as “Super 5”, is a very important surface Al species for both the active site for dehydration reactions and the anchor site for loading catalysts.⁴ For example, the surface Al(V) Lewis acid sites are ascribed to the active sites for alcohol dehydration reaction.^{14,15} It is also suggested that Al(V)s on alumina are the binding sites of active metal atoms such as Pt, Pd, Ru, etc.^{16–20} Indeed, various Al₂O₃ with

abundant Al(V) were synthesized and proved to be good catalysts or catalyst supports.^{21–24} Besides, Al(V) on the surface of γ -Al₂O₃ was also found to be very critical for phase transformation from γ -Al₂O₃ to α -Al₂O₃, which is strongly related to its thermal stability as catalyst support.^{21,25} Theoretical calculations demonstrate that Al(V)s exist on both the (100) surface and microfacets (111) in the reconstructed surface of γ -Al₂O₃.^{26–29} Very recently, it was proposed that the macroscopically defined (110) surfaces in rhombus-platelet γ -Al₂O₃ can be reconstructed into (111) and (100) segments, where Al(V) was derived from six-coordinated Al (Al(VI)) at the (100) surface by removal of hydroxyl groups.³⁰ However, the intrinsic structure related to Al(V) of γ -Al₂O₃ is far from well-known, as it is a very small amount in γ -Al₂O₃, while almost all the reported Al(V)-rich aluminas are in the amorphous phase.

Solid-state NMR spectroscopy is a very powerful tool for exploring the local structure of materials at the atomic level regardless of their crystalline or amorphous properties.^{31–33} Various ²⁷Al NMR techniques including ²⁷Al MAS, ¹H–²⁷Al CP/MAS, ¹H–²⁷Al HMQC, ²⁷Al DQ, and MQ MAS NMR

Received: December 7, 2021

Published: May 23, 2022



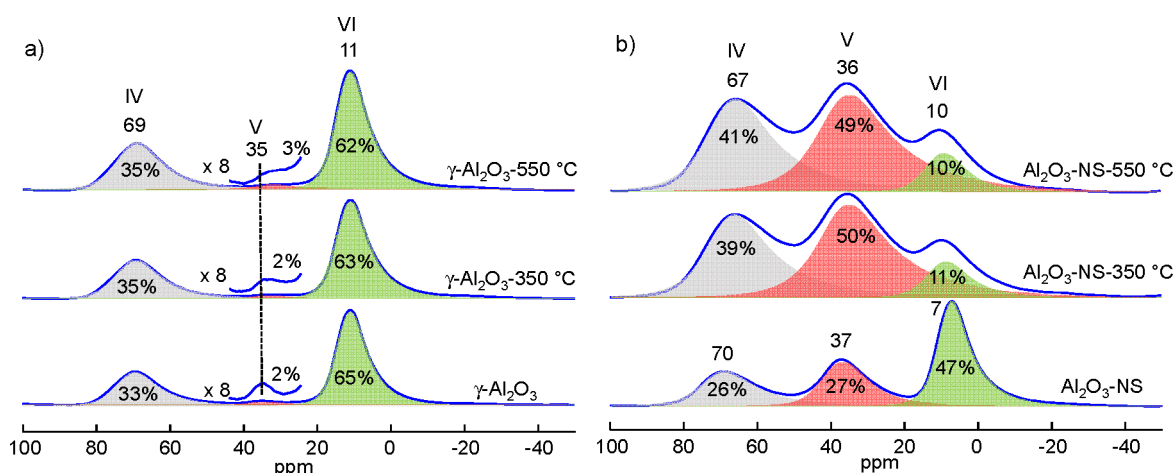


Figure 1. ^{27}Al MAS NMR spectra and the corresponding deconvolutions of pristine (bottom) and dehydrated aluminas at 350 °C (middle) and 550 °C (top), $\gamma\text{-Al}_2\text{O}_3$ (a) and $\text{Al}_2\text{O}_3\text{-NS}$ (b), acquired at 18.8 T and MAS rate of 20 kHz. Note that the absolute errors for the deconvolution are $\pm 0.2\%$ for Al(V) and $\pm 1\%$ for Al(V, VI) in $\gamma\text{-Al}_2\text{O}_3$, while for $\text{Al}_2\text{O}_3\text{-NS}$, the absolute errors are about $\pm 3\%$ due to the spectral overlap.

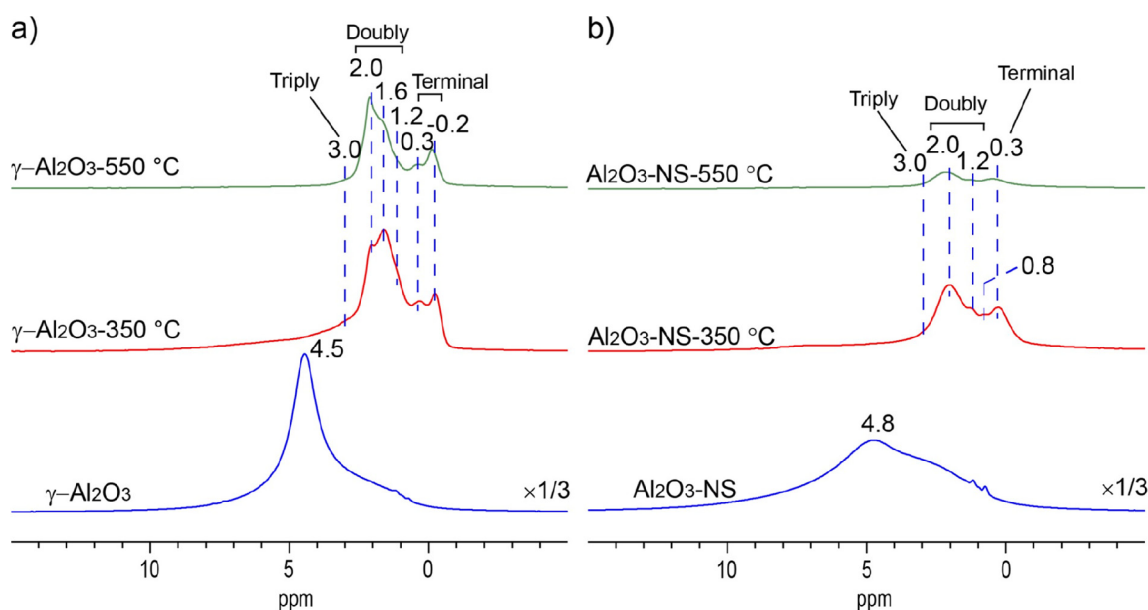


Figure 2. ^1H MAS NMR spectra of pristine (bottom) and dehydrated aluminas at 350 °C (middle) and 550 °C (top), $\gamma\text{-Al}_2\text{O}_3$ (a) and $\text{Al}_2\text{O}_3\text{-NS}$ (b), recorded at 18.8 T and MAS rate of 20 kHz.

have been used to study alumina materials.^{4,34} For commonly used $\gamma\text{-Al}_2\text{O}_3$, Al(V) presents only on the surface and in a very small amount, and its contribution to the signals in the one-pulse ^{27}Al MAS NMR spectra is negligible and difficult to study in detail.³⁵ Recently, it was reported that $^1\text{H}\text{-}^{27}\text{Al}$ HMQC or CP/MAS NMR can significantly enhance the signals of Al(V), and two kinds of Al(V) species with significantly different quadrupolar coupling constants (Q_{cc}) (10 MHz Vs 1–3 MHz) were proposed.^{36–38} However, suffering from low intensity and spectral broadening for ^{27}Al NMR, very few detailed studies on the intrinsic structures related to these Al(V) species have been reported. With the advance of ultra-high-field NMR technology, the detection sensitivity and spectral resolution of the quadrupolar nucleus can be significantly enhanced, providing an opportunity for detailed characterization of Al(V).

Herein, we carried out a comparative investigation on Al(V)-rich $\text{Al}_2\text{O}_3\text{-NS}$ and $\gamma\text{-Al}_2\text{O}_3$ thermally treated under

conditions similar to their practical applications, to elucidate the structural characteristics of Al(V) in $\gamma\text{-Al}_2\text{O}_3$. Benefiting from the significantly enhanced sensitivity and resolution of the ultra-high field up to 35.2 T, $^{27}\text{Al}\text{-}^{27}\text{Al}$ DQ/SQ correlation NMR experiments allowed us to explore direct Al–O–Al connections on the surface of $\gamma\text{-Al}_2\text{O}_3$. By using advanced multinuclear and multidimensional MAS NMR techniques, surprisingly similar features regarding the coordination environment of surface Als and their corresponding hydroxyl groups, selective removal of hydroxyl groups, as well as the distribution of Al(V), were unraveled for $\gamma\text{-Al}_2\text{O}_3$ and $\text{Al}_2\text{O}_3\text{-NS}$.

RESULTS AND DISCUSSION

TEM images and XRD patterns of $\gamma\text{-Al}_2\text{O}_3$ and $\text{Al}_2\text{O}_3\text{-NS}$ are shown in Figure S1 and S2, respectively. $\gamma\text{-Al}_2\text{O}_3$ shows irregular aggregates of nanocrystals, and $\text{Al}_2\text{O}_3\text{-NS}$ shows a long thin sheet morphology as the amorphous phase similar to

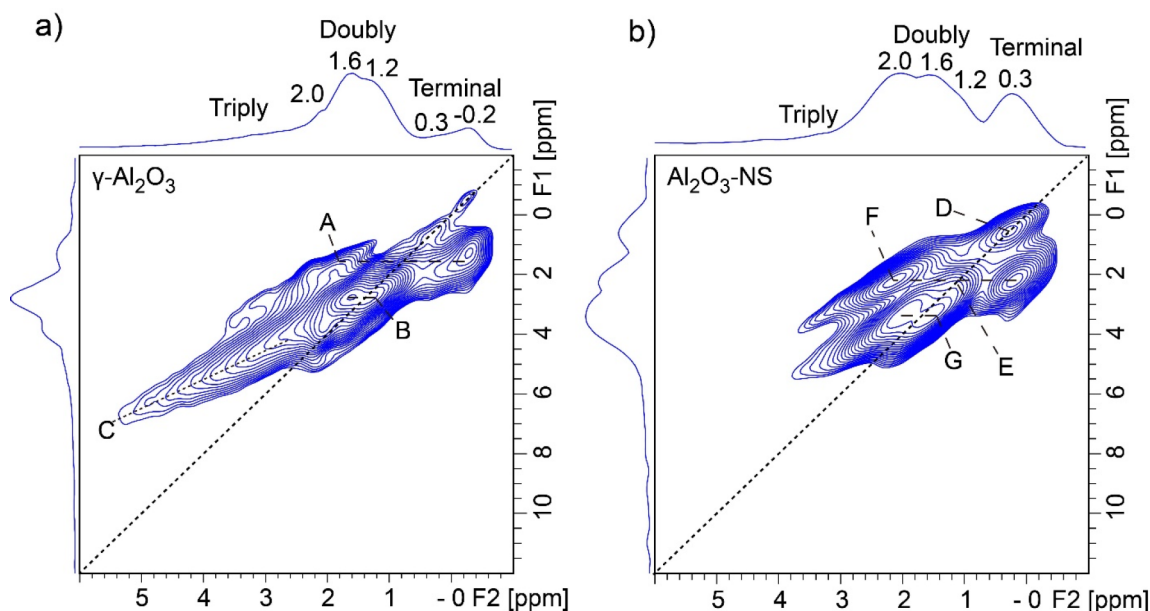


Figure 3. ^1H - ^1H DQ/SQ correlation NMR spectra of 350 °C dehydrated $\gamma\text{-Al}_2\text{O}_3$ (a) and $\text{Al}_2\text{O}_3\text{-NS}$ (b) acquired at 18.8 T and MAS rate of 20 kHz. The BABA sequence was used for ^1H - ^1H dipolar recoupling, and the mixing time was 0.4 ms.

previous reports.³⁹ ^{27}Al MAS NMR spectra of $\gamma\text{-Al}_2\text{O}_3$ and $\text{Al}_2\text{O}_3\text{-NS}$ before and after dehydration at different temperatures and the relative amount of each Al species analyzed by dmfit software according to ^{27}Al MQ MAS NMR (Figure S3) are shown in Figure 1.⁴⁰ The pristine $\gamma\text{-Al}_2\text{O}_3$ (Figure 1a) shows two main peaks at 11 and 69 ppm and minor signals at 35 ppm, corresponding to six(VI)-, four(IV)-, and five(V)-coordinated Al, respectively. After dehydration at 350 and 550 °C, there is only a slight decrease of Al(VI) accompanied by the increase of Al(IV). As only a very small amount of Al(V) is present in $\gamma\text{-Al}_2\text{O}_3$, the quantitative analysis of this Al species is challenging, and opposite trends were reported during the dehydration or preparation of catalysts.^{16,41,42} In contrast, for pristine $\text{Al}_2\text{O}_3\text{-NS}$ (Figure 1b), there is significant signal intensity for the Al(V) at 37 ppm, and the signal of Al(VI) appears at a relatively higher field near 7 ppm. After dehydration at 350 °C, the relative amount of Al(VI) decreases significantly and Al(V) becomes dominant (about 50%). More specifically, the Al(VI) decreases by about 36%, Al(V) and Al(IV) species increase by about 23% and 13%, respectively. The results clearly demonstrate that Al(V) may be formed from the hydration of Al(IV) or dehydration of Al(VI). Although a very small change of the amount of Al(V) for $\gamma\text{-Al}_2\text{O}_3$ was seen, its signal was broadened significantly upon the dehydration treatment (Figures 1a and S3a-c). It suggests that Al(V) is different for $\gamma\text{-Al}_2\text{O}_3$ under different dehydration status, implying some Al(V) was transformed into Al(IV) and also formed from Al(VI) simultaneously.

^1H MAS NMR spectra of pristine and dehydrated Al_2O_3 samples are shown in Figure 2, where the intensity or vertical scale is normalized to the sample weight. The pristine $\gamma\text{-Al}_2\text{O}_3$ and $\text{Al}_2\text{O}_3\text{-NS}$ show signals of hydrogen-bonded and physisorbed water at 4.5 and 4.8 ppm, respectively.⁴¹ After dehydration at 350 °C, for both $\gamma\text{-Al}_2\text{O}_3$ and $\text{Al}_2\text{O}_3\text{-NS}$, three main groups of signals are observed at -0.2 to 0.3, 0.8 to 2.0, and above 2.5 ppm, corresponding to isolated terminal, double-, and triple-bridged hydroxyl groups, respectively.³⁶ It is noted that the major signals of hydroxyl groups in $\text{Al}_2\text{O}_3\text{-NS}$

near 0.3 and 2.0 ppm are also present in $\gamma\text{-Al}_2\text{O}_3$. However, the relative intensities are different, and specifically, the major signal of the terminal hydroxyl locates at 0.3 ppm for $\text{Al}_2\text{O}_3\text{-NS}$ but -0.2 ppm for $\gamma\text{-Al}_2\text{O}_3$, and the main double-bridged hydroxyl groups present at 2.0 ppm for $\text{Al}_2\text{O}_3\text{-NS}$ but 1.6 ppm for $\gamma\text{-Al}_2\text{O}_3$. When elevating the dehydration temperature to 550 °C, most hydroxyl groups (~70% according to integrated area compared with 350 °C dehydrated sample) were desorbed for $\text{Al}_2\text{O}_3\text{-NS}$. On the contrary, only the signals at 0.3, 1.6, and ~3.0 ppm hydroxyl groups on $\gamma\text{-Al}_2\text{O}_3$ decrease apparently. The results clearly indicate that the surface hydroxyl groups in $\gamma\text{-Al}_2\text{O}_3$ have significantly different thermal stability, although the overall stability is much better than those of amorphous $\text{Al}_2\text{O}_3\text{-NS}$.

In order to probe the spatial distribution of different hydroxyl groups on the alumina surface, ^1H - ^1H DQ/SQ correlation NMR experiments were further carried out, and the spectra are shown in Figure 3. The correlation peaks mean that the spin pairs have close spatial proximity. It is worth noting that the terminal hydroxyl groups (-0.2 to 0.3 ppm) in $\gamma\text{-Al}_2\text{O}_3$ show very weak autocorrelation signals (i.e., signals arising from chemically equivalent species in close proximity) along with the diagonal, and a very weak correlation peak (2.0 ppm, 0.3 ppm) was also observed. Three strong correlation peaks between terminal hydroxyl and double-bridged hydroxyl groups (A: -0.2 to 0.3 ppm, 1.6 ppm), double-bridged and double-bridged hydroxyls (B: 1.2 ppm, 1.6 ppm), as well as triple-bridged hydroxyl groups and double-bridged hydroxyl (C: 2.5-5 ppm, 1.6 ppm) are observed. The results demonstrate that the double-bridged hydroxyl at 1.6 ppm correlated with all the other hydroxyl groups in $\gamma\text{-Al}_2\text{O}_3$. As for $\text{Al}_2\text{O}_3\text{-NS}$, strong autocorrelation peaks were observed for terminal (D: 0.3 ppm, 0.3 ppm) and double-bridged hydroxyl groups (E: 1.2 ppm, 1.2 ppm). In addition, the spatial proximities between the terminal hydroxyl and bridged hydroxyl groups (F: 2.0 ppm, 0.3 ppm) and double-bridged hydroxyl groups (G: 1.6 ppm, 2.0 ppm) were observed. It is worth noting that both samples show strong correlations for

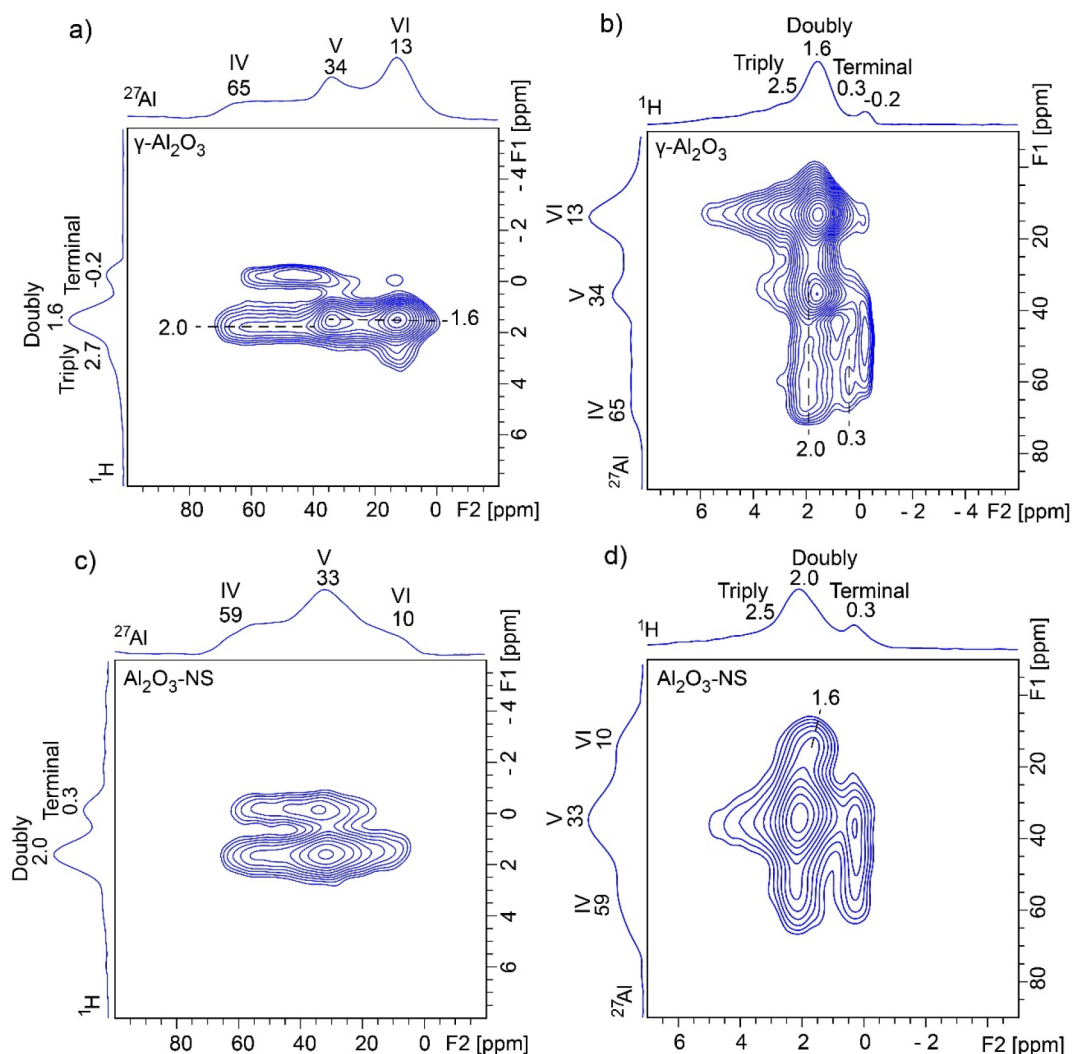


Figure 4. ^1H – ^{27}Al D-RINEPT correlation NMR spectra of $350\text{ }^\circ\text{C}$ dehydrated $\gamma\text{-Al}_2\text{O}_3$ (a,b) and $\text{Al}_2\text{O}_3\text{-NS}$ (c,d) using ^{27}Al (left) and ^1H (right) detection acquired at 18.8 T and MAS rate of 20 kHz. The dipolar recoupling SR4_1^2 sequence was applied during the mixing periods, and the optimized recoupling times were 0.6 and 1.0 ms for ^{27}Al and ^1H detected D-RINEPT NMR experiments, respectively.

the signals near 1.2–2.0 ppm (B and G), which means that these double-bridged hydroxyl groups have close spatial proximity to each other. The proximity of hydroxyl groups may accommodate the dehydration process at high temperatures. For instance, the hydroxyl groups at 1.2–1.6 ppm are mainly hydroxyl groups removed after $550\text{ }^\circ\text{C}$ dehydration for $\gamma\text{-Al}_2\text{O}_3$, as shown in Figure 2a. This is also the case for $\text{Al}_2\text{O}_3\text{-NS}$, where most hydroxyl groups were removed after $550\text{ }^\circ\text{C}$ dehydration, due to the spatial proximity for all of them.

The information on connectivity between hydroxyl groups and surface Al species can be obtained by performing 2D ^1H – ^{27}Al correlation NMR spectroscopy, where the through-space D-RINEPT (refocused insensitive nuclei enhanced by polarization transfer)^{43,44} method was used. Both ^{27}Al and ^1H detected ^1H – ^{27}Al D-RINEPT NMR spectra were acquired, as shown in Figure 4. ^{27}Al detected ^1H – ^{27}Al D-RINEPT spectrum of dehydrated $\gamma\text{-Al}_2\text{O}_3$ (Figure 4a) indicates that the terminal hydroxyl groups at -0.2 ppm correlate with Al(IV), and the double-bridged hydroxyl groups at 1.6 ppm correlate with Al(V) and Al(VI), while the double-bridged hydroxyl groups near 2.0 ppm correlate with Al(IV). The triple-bridged hydroxyl groups above 2.5 ppm are mainly

correlated with Al(VI). These results are consistent with previous reports.³⁶ Thanks to the higher sensitivity and resolution of ^1H dimension in the ^1H detected D-RINEPT spectrum (Figure 4b), additional correlations can be unambiguously discriminated between terminal hydroxyl groups at 0.3 ppm and Al(IV). Moreover, the correlation peak between triple-bridged hydroxyl groups above 2.5 ppm and Al(V) was also observed. In comparison, on the surface of $\text{Al}_2\text{O}_3\text{-NS}$ (Figure 4c), the terminal hydroxyl groups at 0.3 ppm correlate with both Al(IV) and Al(V), while double-bridged hydroxyl groups at 2.0 ppm correlate with all Al(IV), Al(V), and Al(VI), whereas the ^1H detected D-RINEPT spectrum (Figure 4d) shows that the double-bridged hydroxyl groups at 1.6 ppm mainly correlate with Al(VI) and the triple-bridged hydroxyl groups above 2.5 ppm mainly correlate with Al(V). It is worth noting that all the hydroxyl–aluminum correlations in $\text{Al}_2\text{O}_3\text{-NS}$ are observable in $\gamma\text{-Al}_2\text{O}_3$ (clearly shown in ^1H detected D-RINEPT spectra Figure 4b and d), and the only difference is that they have different relative intensities, whereas ^1H – ^{27}Al D-RINEPT spectra of both pristine samples (Figure S4) indicate that surface Al(IV) and

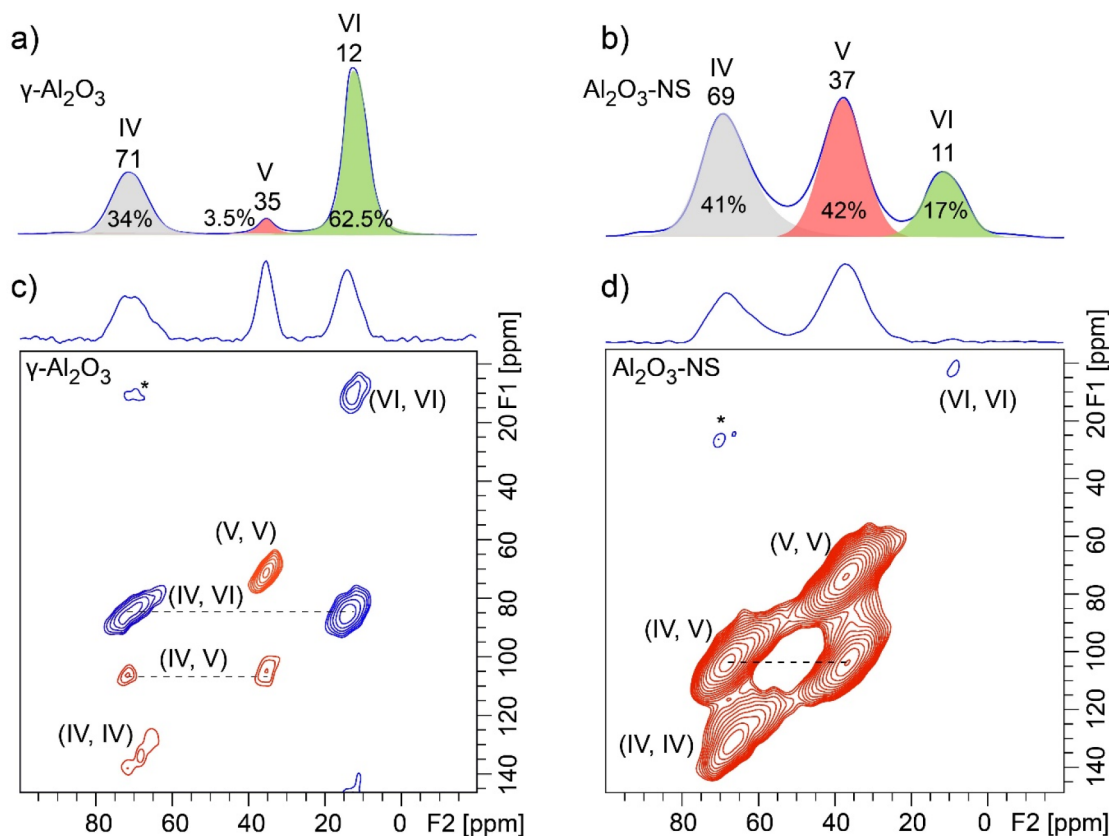


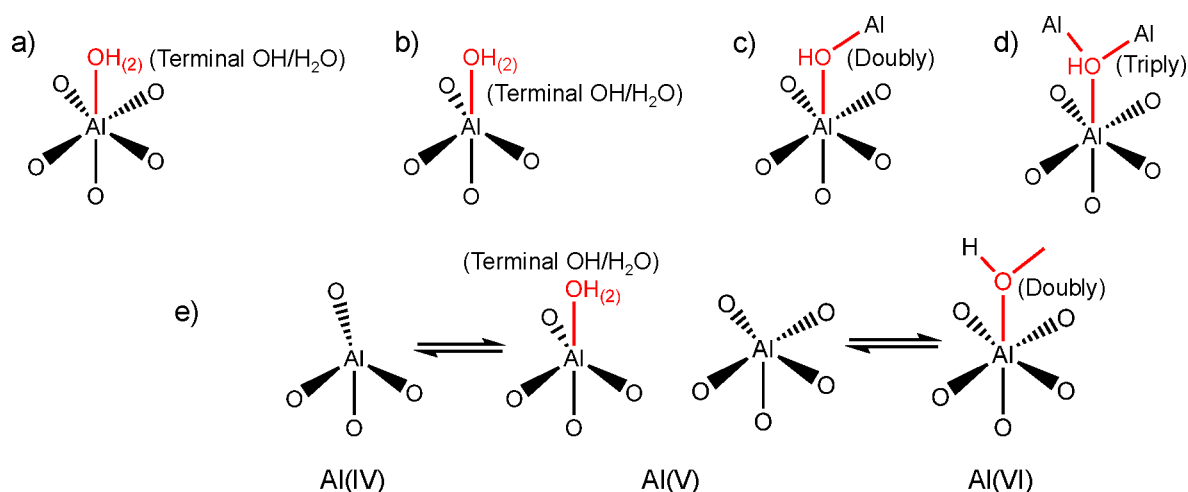
Figure 5. Ultra-high-field 2D ^{27}Al – ^{27}Al DQ/SQ correlation (bottom) and corresponding 1D ^{27}Al MAS NMR spectra (top) of 350 °C dehydrated $\gamma\text{-Al}_2\text{O}_3$ (a,c) and $\text{Al}_2\text{O}_3\text{-NS}$ (b,d) acquired at 35.2 T and MAS rate of 30 kHz. The BR_2^1 sequence with RF field strength of 15 kHz was used for ^{27}Al – ^{27}Al dipolar recoupling, and the recoupling time was 0.8 ms.

Al(V) show similar features with significantly narrower ^{27}Al peaks due to smaller Q_{CC} .

In order to obtain the information on the connectivity of Al with different coordination environments for pristine and dehydrated Al_2O_3 , ^{27}Al – ^{27}Al DQ/SQ NMR experiments were further carried out. It should be noted that ^{27}Al – ^{27}Al DQ/SQ NMR signals are very sensitive to Al–Al distance (see Figure S5 for details). As shown in ^{27}Al – ^{27}Al DQ/SQ NMR spectra of $\gamma\text{-Al}_2\text{O}_3$ with different RF carrier frequencies (Figure S6a–c), although the DQ excitation efficiency is also affected by the carrier frequency, it can still be concluded that Al(VI) was spatially correlated with Al(IV), indicative of the off-diagonal peaks, and also strongly autocorrelated, indicative of the diagonal peak. In contrast to the previous report, the weak correlation among Al(IV) was also observed when the center of RF was moved near Al(IV).⁴⁵ The absence of all correlation peaks related to Al(V) may be due to its very small amount in $\gamma\text{-Al}_2\text{O}_3$ and large quadrupolar interaction. In comparison, ^{27}Al – ^{27}Al DQ/SQ NMR spectrum of $\text{Al}_2\text{O}_3\text{-NS}$ (Figure S6d–f) demonstrates that each aluminum species has autocorrelation, and the correlations with the other two Al species, similar to previously reported Al(V)-rich amorphous mesoporous alumina utilizing the dynamic nuclear polarization (DNP) technique.⁴⁶ It means that all the connectivities among Al(VI), Al(V), and Al(IV) exist for amorphous mesoporous alumina and $\text{Al}_2\text{O}_3\text{-NS}$, but the question whether Al(V) on the surface of $\gamma\text{-Al}_2\text{O}_3$ has similar features as $\text{Al}_2\text{O}_3\text{-NS}$ remains to be answered. In order to have efficient NMR sensitivity and resolution, we further carried out ^{27}Al MAS and DQ/SQ NMR experiments for dehydrated $\gamma\text{-Al}_2\text{O}_3$ and

$\text{Al}_2\text{O}_3\text{-NS}$ at the currently accessible highest field (35.2 T) spectrometer, and the corresponding spectra are shown in Figure 5. As shown in 1D ^{27}Al MAS NMR spectra (Figure 5a,b), the significantly enhanced spectral resolution was achieved at the ultrahigh magnetic field. Note that the five-coordinated Al takes 3.5% ($\pm 0.2\%$) of total Als $\gamma\text{-Al}_2\text{O}_3$, which is slightly different from that derived at 18.8T (Figure 1), and the similar slight deviation was observed for $\text{Al}_2\text{O}_3\text{-NS}$. It should be expected that the significantly improved spectral resolution at ultra-high field can lead to higher accuracy on quantitative analysis. For the ^{27}Al – ^{27}Al DQ/SQ spectrum (Figure 5c), autocorrelations of Al(IV) and Al(VI) and correlation between Al(IV) and Al(VI) from bulk phase were observed to be similar to that of pristine $\gamma\text{-Al}_2\text{O}_3$. Surprisingly, Al(V) in $\gamma\text{-Al}_2\text{O}_3$ presents a strong autocorrelation peak comparable to much more abundant Al(IV) and Al(VI), even though it only accounts for 3.5% of the total Al (Figure 5a), which was never observed even using the DNP NMR technique.³⁵ In addition, the correlation peak between Al(V) and Al(IV) is also observed. Note that with the RF carrier frequency closer to Al(VI), the correlation peaks with Al(VI) become stronger, and the weak correlation between Al(V) and Al(VI) can also be observed (Figure S7). For dehydrated $\text{Al}_2\text{O}_3\text{-NS}$, the ^{27}Al – ^{27}Al DQ/SQ NMR experiment (Figure 5d) demonstrates that Al(V) and Al(IV) have strong autocorrelation signals, as well as a strong correlation between them. However, weak autocorrelation peaks were barely observed for Al(VI) due to the resonance offset. Compared with the ^{27}Al 1D MAS NMR spectra of $\gamma\text{-Al}_2\text{O}_3$ and $\text{Al}_2\text{O}_3\text{-NS}$, there is a significant enhancement of ^{27}Al DQ

Scheme 1. Proposed Models for the Formation of Five-Coordinated Al



MAS NMR signals of Al(V) for γ -Al₂O₃ but not for Al₂O₃-NS, although the RF carrier frequencies for both samples are the same. Therefore, the RF carrier frequency does not play a dominant role at this point. Since Al(V) were proposed to only exist on the surface of γ -Al₂O₃, the presence of these correlation peaks of surface Al species (Al(V)-Al(V), Al(V)-Al(IV), Al(V)-Al(VI)) highly suggests that these spin pairs have closer spatial proximity than those in the bulk phase. It is in accordance with previous reports that the enhanced contrast of surface in TEM images was due to the modified surface structures with excess cations (more dense Al³⁺) at the surface of γ -Al₂O₃.⁴⁷ These ²⁷Al-²⁷Al DQ/SQ NMR results clearly illustrate that Al(V) in γ -Al₂O₃ have the same characteristics as Al₂O₃-NS with respect to Al connectivities (highlighted by red in Figure 5); that is, Al(V)s are spatially autocorrelated and also correlated with Al(IV).

¹H-¹H DQ/SQ and ¹H-²⁷Al D-RINEPT NMR demonstrate that the connectivities between Al and hydroxyl of γ -Al₂O₃ contain all the features that are present on Al₂O₃-NS. ²⁷Al-²⁷Al DQ/SQ NMR results suggest that the Al-O-Al connectivities found in Al₂O₃-NS (highlighted by red in Figure 5) are also included in γ -Al₂O₃ excluding bulk Al(VI)-Al(VI) and Al(IV)-Al(VI) connectivities. All these results allow us to infer that the surface structures related to Al(V) in γ -Al₂O₃ should be similar to those in Al₂O₃-NS. For both γ -Al₂O₃ and Al₂O₃-NS, various Al(V)s should exist: (1) Al(V) from Al(IV) due to adsorption of water; (2) Al(V) from Al(VI) after dehydration by removing bridged hydroxyls. Possible models for the formation of Al(V)s are demonstrated in Scheme 1a-e, while only Al(V)s with smaller quadrupolar interaction are observed in ²⁷Al MQ MAS NMR (Figure S3). Two kinds of Al(V)s were proposed from ¹H-²⁷Al HMQC/CP MAS NMR, i.e., one with strong quadrupolar interaction (10 MHz); the other with weak quadrupolar interaction (1-3 MHz) for dehydrated γ -Al₂O₃.^{36,38} Theoretically, Al(V)s with square pyramidal structure are mainly present on the surface of (100), where only Al(V)s were exposed.^{28,30} Al(V)-O-Al(V) (derived from Al(VI) by dehydration with the shortest Al-Al distance, Scheme 1a) connectivities at the surface of (100) can well explain the strong autocorrelation of five-coordinated Al in ²⁷Al-²⁷Al DQ/SQ NMR. If Al(V)s with square pyramidal structure were mainly derived from the dehydration of surface Al(VI)s with terminal hydroxyl groups after dehydration above

375 °C as previously reported,³⁰ the correlation peaks between Al(VI) and terminal hydroxyl groups should be clearly observed in ¹H-²⁷Al D-RINEPT NMR at moderate dehydration temperature of 350 °C. On the contrary, the ¹H-²⁷Al D-RINEPT NMR results indicate that the terminal hydroxyl groups are mainly correlated with Al(IV) and Al(V) (Figure 4). In fact, Al(V) species with high symmetry were proposed to exist and even observed in liquid solutions, and they are also stable on the surface of hydrated alumina.⁴⁸⁻⁵⁰ Al(V) in γ -Al₂O₃ exposed at ambient conditions might be mainly from the Al(IV) after adsorption of water (Scheme 1b), which shows symmetric signals in ²⁷Al MAS NMR (Figure 1 and Figure S4). The surface reconstruction via the removal of bridged hydroxyl groups of Al(VI)s also forms Al(V)s (Scheme 1c,d) with strong quadrupolar interactions (Figure 1 and Figure 4) on γ -Al₂O₃, which should be another reasonable explanation for the formation of the Al(V) dominant structure upon the dehydration, as revealed by ¹H MAS NMR and predicted by theoretical calculations.⁵¹ As is clearly shown in ²⁷Al MAS NMR, the dehydration treatment leads to the structural reconstruction in Al₂O₃-NS, where about 77% Al(VI) was transformed into Al(IV)/Al(V). Once most of the hydroxyl groups were removed, no significant changes of Al coordination status were observed upon further dehydration even at 550 °C. Moreover, when Al₂O₃-NS was wetted by water, almost all the Al(IV)s and Al(V)s could be transformed into Al(VI) (Figure S8). The flexibility of Al coordination for Al(V)-rich alumina was also previously reported for ρ -alumina, which was too sensitive to moisture to be transformed into hydroxides and oxyhydroxides with Al(VI).^{4,52} It was further confirmed by ¹H-²⁷Al D-RINEPT spectra that the surface Al experience significantly different quadrupolar interactions for both samples in pristine and dehydrated status (Figures 4 and S4). Therefore, the structures of most Al(V) at the surface of γ -Al₂O₃ are highly similar to the Al(V) dominant structures such as amorphous Al₂O₃-NS. Indeed, very high Al(V) content was reported on the deposited amorphous Al₂O₃ thin films as well as mechanically milled γ -Al₂O₃.^{21,53,54} In fact, we can roughly estimate that the relative amount of Al(V) on the surface of γ -Al₂O₃ can reach up to 26% via ultra-high-field ¹H-²⁷Al HMQC NMR spectra (Figure S9), which is an appreciable amount of the total surface Al. Our findings on the extraordinary coordination environment, Al(V) related con-

nections, and viable structure reconstruction may confer distinct roles on Al(V) for active sites, binding sites, or as nucleation center for sintering of alumina.^{15,16,25}

CONCLUSIONS

The structural properties of Al(V) species in alumina were comprehensively studied by a combination of high-field multinuclear and multidimensional MAS NMR. The results demonstrate that amorphous Al₂O₃-NS can be a representative phase to the commonly observed surface Al(V) in γ -Al₂O₃. Quantitative ²⁷Al MAS NMR indicates the flexible coordination numbers of Al changing from six, five, to four for both aluminas. ¹H MAS and DQ/SQ NMR data demonstrate the hydroxyl groups on the surface of γ -Al₂O₃ with close spatial proximity that are viable to be removed under high-temperature dehydration resulting in surface structure reconstruction. Moreover, it is evidenced for the first time that most Al(V) species tend to aggregate into Al(V) domains on the surface of γ -Al₂O₃ like Al₂O₃-NS, rather than tetragonal pyramid coordination on the (100) surface previously predicted from theoretical models. It is believed that these new insights into surface Al(V) species would help to understand the structure–function relationship of Al₂O₃ when used as catalyst and catalyst supports.

ASSOCIATED CONTENT

Supporting Information

The Supporting Information is available free of charge at <https://pubs.acs.org/doi/10.1021/acscentsci.1c01497>.

XRD patterns, TEM images, ²⁷Al MAS and MQ MAS NMR spectra, 1D ¹H–²⁷Al HMQC MAS NMR, ²⁷Al–²⁷Al DQ MAS NMR spectra (PDF)

AUTHOR INFORMATION

Corresponding Author

Guangjin Hou – State Key Laboratory of Catalysis, Dalian Institute of Chemical Physics, Chinese Academy of Sciences, Dalian 116023, China; orcid.org/0000-0001-8216-863X; Email: g hou@dicp.ac.cn

Authors

Zhenchao Zhao – State Key Laboratory of Catalysis, Dalian Institute of Chemical Physics, Chinese Academy of Sciences, Dalian 116023, China

Dong Xiao – State Key Laboratory of Catalysis, Dalian Institute of Chemical Physics, Chinese Academy of Sciences, Dalian 116023, China; orcid.org/0000-0003-1485-4915

Kuizhi Chen – State Key Laboratory of Catalysis, Dalian Institute of Chemical Physics, Chinese Academy of Sciences, Dalian 116023, China; National High Magnetic Field Laboratory, Tallahassee, Florida 32310, United States; orcid.org/0000-0002-9853-7070

Rui Wang – State Key Laboratory of Catalysis, Dalian Institute of Chemical Physics, Chinese Academy of Sciences, Dalian 116023, China

Lixin Liang – State Key Laboratory of Catalysis, Dalian Institute of Chemical Physics, Chinese Academy of Sciences, Dalian 116023, China

Zhengmao Liu – State Key Laboratory of Catalysis, Dalian Institute of Chemical Physics, Chinese Academy of Sciences, Dalian 116023, China; orcid.org/0000-0002-4597-0022

Ivan Hung – National High Magnetic Field Laboratory, Tallahassee, Florida 32310, United States; orcid.org/0000-0001-8916-739X

Zhehong Gan – National High Magnetic Field Laboratory, Tallahassee, Florida 32310, United States; orcid.org/0000-0002-9855-5113

Complete contact information is available at:

<https://pubs.acs.org/10.1021/acscentsci.1c01497>

Notes

The authors declare no competing financial interest.

ACKNOWLEDGMENTS

We are grateful for the financial support from the National Key R&D Program of China (2021YFA1502803), National Natural Science Foundation of China (Nos. 21972143, 22002165, 21773230, 91945302, 21603022, and 21773233), Liao Ning Revitalization Talents Program (XLYC1807207), Dalian Youth Science and Technology Star Program (2019RQ079), DICP&QIBEBT UN201808, and DICP I202104. A portion of this work was performed at the National High Magnetic Field Laboratory, which is supported by the National Science Foundation Cooperative Agreement No. DMR-1644779 and the State of Florida. Development of the SCH magnet and NMR instrumentation was supported by NSF (DMR-1039938 and DMR-0603042) and NIH P41 GM122698.

REFERENCES

- (1) Pines, H.; Haag, W. O. Alumina: Catalyst and Support. I. Alumina, Its Intrinsic Acidity and Catalytic Activity. *J. Am. Chem. Soc.* **1960**, *82*, 2471–2483.
- (2) Trueba, M.; Trasatti, S. P. γ -Alumina as a Support for Catalysts: A Review of Fundamental Aspects. *Eur. J. Inorg. Chem.* **2005**, *2005*, 3393–3403.
- (3) Digne, M.; Sautet, P.; Raybaud, P.; Euzen, P.; Toulhoat, H. Hydroxyl Groups on γ -Alumina Surfaces: A DFT Study. *J. Catal.* **2002**, *211*, 1–5.
- (4) Chandran, C. V.; Kirschhock, C. E. A.; Radhakrishnan, S.; Taulelle, F.; Martens, J. A.; Breynaert, E. Alumina: Discriminative Analysis Using 3D Correlation of Solid-State NMR Parameters. *Chem. Soc. Rev.* **2019**, *48*, 134–156.
- (5) Boumaza, A.; Favaro, L.; Lédion, J.; Sattonnay, G.; Brubach, J. B.; Berthet, P.; Huntz, A. M.; Roy, P.; Tétot, R. Transition Alumina Phases Induced by Heat Treatment of Boehmite: An X-Ray Diffraction and Infrared Spectroscopy Study. *J. Solid State Chem.* **2009**, *182*, 1171–1176.
- (6) Joubert, J.; Fleurat-Lessard, P.; Delbecq, F.; Sautet, P. Simulating Temperature Programmed Desorption of Water on Hydrated γ -Alumina from First-Principles Calculations. *J. Phys. Chem. B* **2006**, *110*, 7392–7395.
- (7) Amenomiya, Y.; Cvitanović, R. J. Active Sites of Alumina and Silica-Alumina as Observed by Temperature Programmed Desorption. *J. Catal.* **1970**, *18*, 329–337.
- (8) Kovarik, L.; Genc, A.; Wang, C.; Qiu, A.; Peden, C. H. F.; Szanyi, J.; Kwak, J. H. Tomography and High-Resolution Electron Microscopy Study of Surfaces and Porosity in a Plate-Like γ -Al₂O₃. *J. Phys. Chem. C* **2013**, *117*, 179–186.
- (9) Xu, S.; Jaegers, N. R.; Hu, W.; Kwak, J. H.; Bao, X.; Sun, J.; Wang, Y.; Hu, J. Z. High-Field One-Dimensional and Two-Dimensional ²⁷Al Magic-Angle Spinning Nuclear Magnetic Resonance Study of Θ -, Δ -, and γ -Al₂O₃ Dominated Aluminum Oxides: Toward Understanding the Al Sites in γ -Al₂O₃. *ACS Omega* **2021**, *6*, 4090–4099.
- (10) Wang, Q.; Li, W.; Hung, I.; Mentink-Vigier, F.; Wang, X.; Qi, G.; Wang, X.; Gan, Z.; Xu, J.; Deng, F. Mapping the Oxygen Structure

- of γ -Al₂O₃ by High-Field Solid-State NMR Spectroscopy. *Nat. Commun.* **2020**, *11*, 3620.
- (11) Paglia, G.; Božin, E. S.; Billinge, S. J. L. Fine-Scale Nanostructure in γ -Al₂O₃. *Chem. Mater.* **2006**, *18*, 3242–3248.
- (12) Samain, L.; Jaworski, A.; Edén, M.; Ladd, D. M.; Seo, D.-K.; Javier Garcia-Garcia, F.; Häussermann, U. Structural Analysis of Highly Porous γ -Al₂O₃. *J. Solid State Chem.* **2014**, *217*, 1–8.
- (13) Prins, R. Location of the Spinel Vacancies in γ -Al₂O₃. *Angew. Chem., Int. Ed.* **2019**, *58*, 15548–15552.
- (14) Larmier, K.; Chizallet, C.; Cadran, N.; Maury, S.; Abboud, J.; Lamic-Humblot, A.-F.; Marceau, E.; Lauron-Pernot, H. Mechanistic Investigation of Isopropanol Conversion on Alumina Catalysts: Location of Active Sites for Alkene/Ether Production. *ACS Catal.* **2015**, *5*, 4423–4437.
- (15) Hu, J. Z.; et al. High Field ²⁷Al MAS NMR and TPD Studies of Active Sites in Ethanol Dehydration Using Thermally Treated Transitional Aluminas as Catalysts. *J. Catal.* **2016**, *336*, 85–93.
- (16) Kwak, J. H.; Hu, J.; Mei, D.; Yi, C.-W.; Kim, D. H.; Peden, C. H. F.; Allard, L. F.; Szanyi, J. Coordinatively Unsaturated Al³⁺ Centers as Binding Sites for Active Catalyst Phases of Platinum on γ -Al₂O₃. *Science* **2009**, *325*, 1670–1673.
- (17) Zhang, Z.; et al. Thermally Stable Single Atom Pt/M-Al₂O₃ for Selective Hydrogenation and CO Oxidation. *Nat. Commun.* **2017**, *8*, 16100.
- (18) Duan, H.; You, R.; Xu, S.; Li, Z.; Qian, K.; Cao, T.; Huang, W.; Bao, X. Pentacoordinated Al³⁺-Stabilized Active Pd Structures on Al₂O₃-Coated Palladium Catalysts for Methane Combustion. *Angew. Chem., Int. Ed.* **2019**, *58*, 12043–12048.
- (19) Tang, N.; Cong, Y.; Shang, Q.; Wu, C.; Xu, G.; Wang, X. Coordinatively Unsaturated Al³⁺ Sites Anchored Subnanometric Ruthenium Catalyst for Hydrogenation of Aromatics. *ACS Catal.* **2017**, *7*, 5987–5991.
- (20) Mei, D.; Kwak, J. H.; Hu, J.; Cho, S. J.; Szanyi, J.; Allard, L. F.; Peden, C. H. F. Unique Role of Anchoring Penta-Coordinated Al³⁺ Sites in the Sintering of γ -Al₂O₃-Supported Pt Catalysts. *J. Phys. Chem. Lett.* **2010**, *1*, 2688–2691.
- (21) Düvel, A.; Romanova, E.; Sharifi, M.; Freude, D.; Wark, M.; Heitjans, P.; Wilkening, M. Mechanically Induced Phase Transformation of γ -Al₂O₃ into α -Al₂O₃. Access to Structurally Disordered γ -Al₂O₃ with a Controllable Amount of Pentacoordinated Al Sites. *J. Phys. Chem. C* **2011**, *115*, 22770–22780.
- (22) Chen, S.; Chen, J.; Qu, T.; Xiang, K.; Zhang, Y.; Hao, P.; Peng, L.; Xie, M.; Guo, X.; Ding, W. Crown Ether Induced Assembly to γ -Al₂O₃ Nanosheets with Rich Pentacoordinate Al³⁺ Sites and High Ethanol Dehydration Activity. *Appl. Surf. Sci.* **2018**, *457*, 626–632.
- (23) Yuan, Q.; Yin, A.-X.; Luo, C.; Sun, L.-D.; Zhang, Y.-W.; Duan, W.-T.; Liu, H.-C.; Yan, C.-H. Facile Synthesis for Ordered Mesoporous γ -Aluminas with High Thermal Stability. *J. Am. Chem. Soc.* **2008**, *130*, 3465–3472.
- (24) Shi, L.; Deng, G.-M.; Li, W.-C.; Miao, S.; Wang, Q.-N.; Zhang, W.-P.; Lu, A.-H. Al₂O₃ Nanosheets Rich in Pentacoordinate Al³⁺ Ions Stabilize Pt-Sn Clusters for Propane Dehydrogenation. *Angew. Chem., Int. Ed.* **2015**, *54*, 13994–13998.
- (25) Kwak, J. H.; Hu, J.; Lukaski, A.; Kim, D. H.; Szanyi, J.; Peden, C. H. F. Role of Pentacoordinated Al³⁺ Ions in the High Temperature Phase Transformation of γ -Al₂O₃. *J. Phys. Chem. C* **2008**, *112*, 9486–9492.
- (26) Wischert, R.; Copéret, C.; Delbecq, F.; Sautet, P. Optimal Water Coverage on Alumina: A Key to Generate Lewis Acid–Base Pairs That Are Reactive Towards the C-H Bond Activation of Methane. *Angew. Chem., Int. Ed.* **2011**, *50*, 3202–3205.
- (27) Wischert, R.; Laurent, P.; Copéret, C.; Delbecq, F.; Sautet, P. γ -Alumina: The Essential and Unexpected Role of Water for the Structure, Stability, and Reactivity of “Defect” Sites. *J. Am. Chem. Soc.* **2012**, *134*, 14430–14449.
- (28) Digne, M.; Sautet, P.; Raybaud, P.; Euzen, P.; Toulhoat, H. Use of DFT to Achieve a Rational Understanding of Acid–Basic Properties of γ -Alumina Surfaces. *J. Catal.* **2004**, *226*, 54–68.
- (29) Pinto, H. P.; Nieminen, R. M.; Elliott, S. D. Ab Initio Study of γ -Al₂O₃ Surfaces. *Phys. Rev. B* **2004**, *70*, 125402.
- (30) Khivantsev, K.; Jaegers, N. R.; Kwak, J.-H.; Szanyi, J.; Kovarik, L. Precise Identification and Characterization of Catalytically Active Sites on the Surface of γ -Alumina. *Angew. Chem., Int. Ed.* **2021**, *60*, 17522–17530.
- (31) Bonhomme, C.; Coelho, C.; Baccile, N.; Gervais, C.; Azais, T.; Babonneau, F. Advanced Solid State NMR Techniques for the Characterization of Sol–Gel-Derived Materials. *Acc. Chem. Res.* **2007**, *40*, 738–746.
- (32) Ashbrook, S. E.; Hodgkinson, P. Perspective: Current Advances in Solid-State NMR Spectroscopy. *J. Chem. Phys.* **2018**, *149*, 040901.
- (33) Li, S.; Lafon, O.; Wang, W.; Wang, Q.; Wang, X.; Li, Y.; Xu, J.; Deng, F. Recent Advances of Solid-State NMR Spectroscopy for Microporous Materials. *Adv. Mater.* **2020**, *32*, 2002879.
- (34) O’Dell, L. A.; Savin, S. L. P.; Chadwick, A. V.; Smith, M. E. A ²⁷Al MAS NMR Study of a Sol–Gel Produced Alumina: Identification of the NMR Parameters of the Θ -Al₂O₃ Transition Alumina Phase. *Solid State Nucl. Magn. Reson.* **2007**, *31*, 169–173.
- (35) Lee, D.; Duong, N. T.; Lafon, O.; De Paëpe, G. Primostrato Solid-State NMR Enhanced by Dynamic Nuclear Polarization: Pentacoordinated Al³⁺ Ions Are Only Located at the Surface of Hydrated γ -Alumina. *J. Phys. Chem. C* **2014**, *118*, 25065–25076.
- (36) Taoufik, M.; Szeto, K. C.; Merle, N.; Rosal, I. D.; Maron, L.; Trébosc, J.; Tricot, G.; Gauvin, R. M.; Delevoye, L. Heteronuclear NMR Spectroscopy as a Surface-Selective Technique: A Unique Look at the Hydroxyl Groups of γ -Alumina. *Chem.—Eur. J.* **2014**, *20*, 4038–4046.
- (37) Szeto, K. C.; Merle, N.; Trébosc, J.; Taoufik, M.; Gauvin, R. M.; Pourpoint, F.; Delevoye, L. Caveat on the Actual Robustness of Heteronuclear NMR Methods for Probing the Surface of γ -Alumina and Related Catalysts. *J. Phys. Chem. C* **2019**, *123*, 12919–12927.
- (38) Wischert, R.; Florian, P.; Copéret, C.; Massiot, D.; Sautet, P. Visibility of Al Surface Sites of γ -Alumina: A Combined Computational and Experimental Point of View. *J. Phys. Chem. C* **2014**, *118*, 15292–15299.
- (39) Wang, J.; Lu, A.-H.; Li, M.; Zhang, W.; Chen, Y.-S.; Tian, D.-X.; Li, W.-C. Thin Porous Alumina Sheets as Supports for Stabilizing Gold Nanoparticles. *ACS Nano* **2013**, *7*, 4902–4910.
- (40) Massiot, D.; Fayon, F.; Capron, M.; King, I.; Le Calvé, S.; Alonso, B.; Durand, J.-O.; Bujoli, B.; Gan, Z.; Hoatson, G. Modelling One- and Two-Dimensional Solid-State NMR Spectra. *Magn. Reson. Chem.* **2002**, *40*, 70–76.
- (41) Shen, L.; Wang, Y.; Du, J.-H.; Chen, K.; Lin, Z.; Wen, Y.; Hung, I.; Gan, Z.; Peng, L. Probing Interactions of γ -Alumina with Water Via Multinuclear Solid-State NMR Spectroscopy. *ChemCatChem* **2020**, *12*, 1569–1574.
- (42) Wang, F.; Ma, J.; Xin, S.; Wang, Q.; Xu, J.; Zhang, C.; He, H.; Cheng Zeng, X. Resolving the Puzzle of Single-Atom Silver Dispersion on Nanosized γ -Al₂O₃ Surface for High Catalytic Performance. *Nat. Commun.* **2020**, *11*, 529.
- (43) Bax, A. Structure Determination and Spectral Assignment by Pulsed Polarization Transfer Via Long-Range ¹H ¹³C Couplings. *J. Magn. Reson.* **1984**, *57*, 314–318.
- (44) Amoureux, J. P.; Trebosc, J.; Wiench, J.; Pruski, M. HMQC and Refocused-Inept Experiments Involving Half-Integer Quadrupolar Nuclei in Solids. *J. Magn. Reson.* **2007**, *184*, 1–14.
- (45) Iuga, D. Double-Quantum Homonuclear Correlations of Spin I = 5/2 Nuclei. *J. Magn. Reson.* **2011**, *208*, 225–234.
- (46) Lee, D.; Takahashi, H.; Thankamony, A. S. L.; Dacquain, J.-P.; Bardet, M.; Lafon, O.; De Paëpe, G. Enhanced Solid-State NMR Correlation Spectroscopy of Quadrupolar Nuclei Using Dynamic Nuclear Polarization. *J. Am. Chem. Soc.* **2012**, *134*, 18491–18494.
- (47) Rozita, Y.; Brydson, R.; Scott, A. J. An Investigation of Commercial Gamma-Al₂O₃ Nanoparticles. *J. Phys.: Conf. Ser.* **2010**, *241*, 012096.
- (48) Swaddle, T. W.; Rosenqvist, J.; Yu, P.; Bylaska, E.; Phillips, B. L.; Casey, W. H. Kinetic Evidence for Five-Coordination in AlOH(Aq)²⁺ Ion. *Science* **2005**, *308*, 1450–1453.

(49) Taulelle, F.; Pruski, M.; Amoureux, J. P.; Lang, D.; Bailly, A.; Huguenard, C.; Haouas, M.; Gérardin, C.; Loiseau, T.; Férey, G. Isomerization of the Prenucleation Building Unit During Crystallization of $\text{AlPO}_4\text{-CJ}_2$: An MQMAS, CP-MQMAS, and HETCOR NMR Study. *J. Am. Chem. Soc.* **1999**, *121*, 12148–12153.

(50) Ahrem, L.; Scholz, G.; Gutmann, T.; Calvo, B.; Buntkowsky, G.; Kemnitz, E. Direct Observation of Coordinatively Unsaturated Sites on the Surface of a Fluoride-Doped Alumina Catalyst. *J. Phys. Chem. C* **2017**, *121*, 12206–12213.

(51) Prins, R. On the Structure of $\gamma\text{-Al}_2\text{O}_3$. *J. Catal.* **2020**, *392*, 336–346.

(52) Slade, R. C. T.; Southern, J. C.; Thompson, I. M. ^{27}Al Nuclear Magnetic Resonance Spectroscopy Investigation of Thermal Transformation Sequences of Alumina Hydrates. Part 1.—Gibbsite, $\gamma\text{-Al}(\text{OH})_3$. *J. Mater. Chem.* **1991**, *1*, 563–568.

(53) Cui, J. L.; et al. Aluminum Oxide Thin Films from Aqueous Solutions: Insights from Solid-State NMR and Dielectric Response. *Chem. Mater.* **2018**, *30*, 7456–7463.

(54) Sarou-Kanian, V.; Gleizes, A. N.; Florian, P.; Samélor, D.; Massiot, D.; Vahlas, C. Temperature-Dependent 4-, 5- and 6-Fold Coordination of Aluminum in MOCVD-Grown Amorphous Alumina Films: A Very High Field ^{27}Al -NMR Study. *J. Phys. Chem. C* **2013**, *117*, 21965–21971.

Recommended by ACS

Direct Detection of Reactive Gallium-Hydride Species on the Ga_2O_3 Surface via Solid-State NMR Spectroscopy

Hongyu Chen, Guangjin Hou, *et al.*

SEPTEMBER 14, 2022
JOURNAL OF THE AMERICAN CHEMICAL SOCIETY

READ 

Interconversion of Atomically Dispersed Platinum Cations and Platinum Clusters in Zeolite ZSM-5 and Formation of Platinum gem-Dicarbonyls

Noah Felvey, Coleman X. Kronawitter, *et al.*

JULY 19, 2022
JOURNAL OF THE AMERICAN CHEMICAL SOCIETY

READ 

Tracking Sub-Nano-Scale Structural Evolution in Zeolite Synthesis by *In Situ* High-Energy X-ray Total Scattering Measurement with Pair Distribution Function Analysis

Ayano Minami, Toru Wakihara, *et al.*

DECEMBER 16, 2022
JOURNAL OF THE AMERICAN CHEMICAL SOCIETY

READ 

The Extent of Platinum-Induced Hydrogen Spillover on Cerium Dioxide

Arik Beck, Jeroen A. van Bokhoven, *et al.*

DECEMBER 05, 2022
ACS NANO

READ 

Get More Suggestions >